ACS Partner Journal

Journal of the American Society for Mass Spectrometry

pubs.acs.org/jasms

Critical Insight

Propagating Error through Traveling-Wave Ion Mobility Calibration

Alexis N. Edwards, Hien M. Tran, and Elyssia S. Gallagher*

Cite This: *J. Am. Soc. Mass Spectrom.* 2021, 32, 2621−2630

Read Online

ACCESS | Metrics & More | Article Recommendations | Supporting Information

ABSTRACT: Native mass spectrometry (MS) is used to elucidate the stoichiometry of protein complexes and quantify binding interactions by maintaining native-like, noncovalent interactions in the gas phase. However, ionization forces proteins into specific conformations, losing the solution-phase dynamics associated with solvated protein structures. Comparison of gas-phase structures to those in solution, or to other gas-phase ion populations, has many biological implications. For one, analyzing the variety of conformations that are maintained in the gas-phase can provide insight into a protein's solution-phase energy landscape. The gas-phase conformations of proteins and complexes can be investigated using ion mobility (IM) spectrometry. Specifically, drift tube (DT)-IM utilizes uniform electric fields to propel a population of gas-phase ions through a region containing a neutral gas. By measuring the mobility (K) of gas-phase ions, users are able to calculate an average momentum transfer cross section (^{DT}CCS), which provides structural information on the ion. Conversely, in traveling-wave ion mobility spectrometry (TWIMS), ^{TW}CCS values cannot be derived directly from an ion's mobility but must be determined following calibration. Though the required calibration adds uncertainty, it is common to report only an average and standard deviation of the calculated ^{TW}CCS, accounting for uncertainty associated with replicate measurements, which is a fraction of the overall uncertainty. Herein, we calibrate a TWIMS instrument and derive ^{TW}CCS$_{N2}$ and ^{TW}CCS$_{N2\rightarrow He}$ values for four proteins: cytochrome *c*, ubiquitin, apo-myoglobin, and holo-myoglobin. We show that compared to reporting only the standard deviation of ^{TW}CCS, propagating error through the calibration results in a significant increase in the number of calculated ^{TW}CCS values that agree within experimental error with literature values (^{DT}CCS). Incorporating this additional uncertainty provides a more thorough assessment of a protein ion's gas-phase conformations, enabling the structures sampled by native IM-MS to be compared against other reported structures, both experimental and computational.

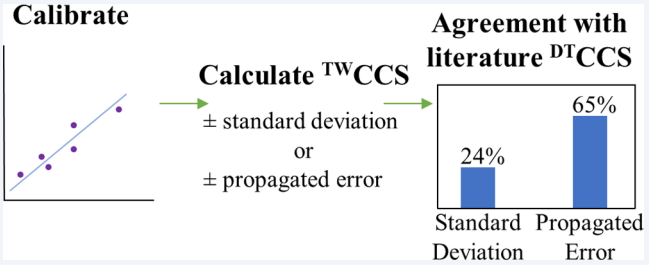

Native mass spectrometry (MS) has become a valuable tool for structural biology, enabling the study of protein complexes and binding interactions,[1,2] DNA assemblies,[3,4] intact viruses,[5] lipid membranes,[6] and transmembrane proteins.[7] These studies have been used to determine the stoichiometry of protein complexes,[8,9] describe the organization of subunits within complexes,[10,11] and quantify binding constants.[12] Yet, each of these studies requires that some degree of higher order structure be preserved in the gas phase for the protein or complex. Thus, in native MS, proteins are sprayed from buffers and aqueous solvents using soft ionization techniques, such as nanoelectrospray (nanoESI), to maintain noncovalent interactions. However, ionization results in proteins losing their dynamic structures and adopting static conformations. While a single gas-phase conformer is not representative of the protein's solution-phase energy landscape, the ability to sample a variety of conformers can provide insight into the dynamic structures that exist in solution.[13,14] Therefore, to characterize the range of structures associated with the observed gas-phase conformers, native MS is regularly coupled to ion mobility spectrometry (IM).

IM allows for the determination of an ion's gas-phase mobility as it travels through a drift gas under an electric field. Gas-phase ions rotate as they move through the drift cell and interact with inert gas molecules, undergoing multiple momentum transfers.[15,16] These interactions include acceleration of the ion via the electric field and deceleration due to opposing resistance, or friction, caused by collisions with the inert buffer gas.[16−18] Collisions with the buffer gas molecules impede the analyte ion's movement, directly affecting the time it takes for the ion to move through the mobility cell. Larger, extended ions interact with the buffer gas more than smaller, condensed structures, resulting in larger ions spending more time in the mobility cell. The momentum transfer that the ion experiences can be averaged to give an average momentum transfer cross section (CCS). This ion-neutral CCS provides information on the size and shape of the ion. Thus, differences in mobility, and by extension CCS, are partially correlated to differences in structure.

Received: April 22, 2021
Revised: September 27, 2021
Accepted: September 30, 2021
Published: October 18, 2021

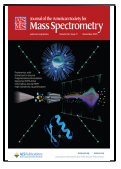

In drift tube (DT)-IM, an ion's mobility (K) through a homogeneous gas is determined by measuring its steady-state velocity (v_d), where t_d is the time that it takes the analyte to travel the length (L) of the mobility cell. The acceleration and deceleration of gas-phase ions have a direct effect on t_d and, by extension, v_d.

$$v_d = \frac{L}{t_d} \tag{1}$$

As the analyte travels through the mobility cell, colliding with inert gas molecules, such as N_2 or He, the ion is under the influence of an electric field (E) that is determined by the magnitude of the voltage (V) across the length of the cell (L).

$$E = \frac{V}{L} \tag{2}$$

Upon considering eqs 1 and 2, K can be written as a ratio between the steady-state velocity of the analyte and the electric field, as shown in eq 3.

$$K = \frac{v_d}{E} \tag{3}$$

An ion's K can then be used to derive a CCS (Ω) using the low-field, ion mobility equation,[17−19] also referred to as the Mason−Schamp equation (eq 4).

$$\Omega = \frac{3}{16}\sqrt{\frac{2\pi}{\mu k_B T}} \times \frac{ze}{NK} \tag{4}$$

Here, μ is the reduced mass of the ion and buffer gas molecules, k_B is the Boltzmann constant, T is the absolute temperature of the drift gas, z is the charge state of the ion, e is the charge of an electron, and N is the drift gas number density.

Equation 4 is an oversimplification of what occurs in an IM experiment and incorporates several assumptions. Many of these assumptions are associated with the effect of collisions between the analyte and buffer gas, which can influence temperature (T). Equation 4 assumes that the electric field (E) is weak.[19] Thus, it is assumed that the energy that the gas-phase ions receive from the electric field is minimal compared to the thermal energy transfer caused by collisions with the buffer gas.[17,19] This means that eq 4 fails to consider how the rate of collisions increases as E increases.[17,19,20] Another assumption is that there are no three-body collisions[21] between the analyte and drift gas, which is unlikely with large analytes, such as proteins. Thermal conductivity of the buffer gas is also ignored. The thermal conductivity of the buffer gas determines its ability to transfer energy[22,23] to the analyte upon collision, which can affect not only T but the three-dimensional structure. Extensive heat transfer can cause unfolding or fragmentation of the analyte.[24−26] As an example, He has a larger thermal conductivity than N_2 and thus produces more heat upon interactions with an analyte,[27] affecting T. The characteristics of the different drift gases are often overlooked as well. Monatomic (e.g., He) and diatomic drift gases (e.g., N_2) have differences in polarizability, which affect analyte mobility due to changes in long-rage interactions.[29−32] Equation 4 also assumes that the drift gas is not a mixture, which affects μ.[18] If the user chooses to utilize a mixed buffer gas, K can be corrected by incorporating the mole fraction of the gases.[18,28] However, for some instruments, such as the Waters Synapt G2-S, unintentional mixing occurs in which the ratio of gases is not known, preventing K from being corrected. While these assumptions are accepted to calculate CCS values with the Mason−Schamp equation, they introduce uncertainty.

There are several opportunities for experimental uncertainties to arise (Figure 1). First, for traditional DT-IM the exact drift cell length must be known, so any uncertainty in the measured length adds uncertainty to K and the calculated CCS values.[33−36] The electric field strength and homogeneity[18] are other critical sources of uncertainty. Equation 4 becomes less accurate as field strength increases. For eq 4, it is assumed that the electric field is weak and has little effect on T compared to the thermal energy experienced by the ions due to collisions with the buffer gas.[19,20] Additionally, increasing E causes the rate of collisions to increase, causing more thermal energy and thus changing T, which would have a compounding effect on the accuracy of K. Therefore, deviations in E affect the accuracy of T and alter the measured K (eq 3), which affects the calculated ion-neutral CCS (eq 4). While it has been estimated that the error caused by uncorrected field strengths is below 10%,[19] this decrease in accuracy prevents comparison of ^{DT}CCS values determined by different research groups and across different platforms. These factors affect the mobility of each ion within the population and increase the uncertainty associated with both the measured mobility and the calculated ^{DT}CCS values.

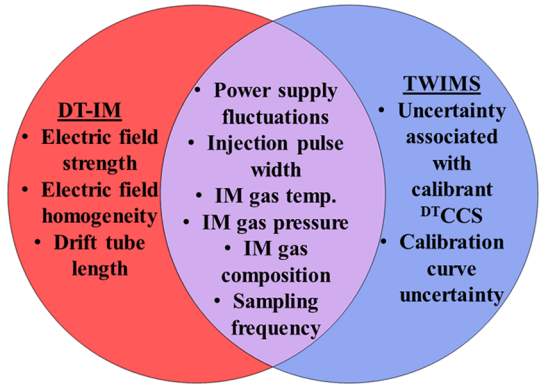

Figure 1. Venn diagram illustrating sources of uncertainty for DT-IM (red) and TWIMS (blue) instruments.

Furthermore, there are sources of uncertainty that affect all IM experiments. Temperature of the drift gas is an important factor for IM experiments as K or CCS are inversely proportional to T. While most instruments allow users to input a value to control T, T is rarely measured in the IM cell. Additionally, as the gas-phase ions collide with the inert buffer gas they experience frictional forces, generating heat, which alters the experimental T. Drift gas pressure[37,38] and power supply voltages[33,34] are extremely important as changes in IM pressure affect frictional drag experienced by the gas-phase ions, and fluctuations in the voltage affect that ion's ability to be propelled through the IM cell. While most instruments allow users to input values for the power supply and gas pressure, fluctuations can occur that affect the measured K value. Ion injection pulse width into the IM cell affects the homogeneity of the ion population and, by extension, broadens the mobility distribution of the ions.[18,39,40] This in turn limits resolving power (R_p), which is a quantification of ion separation defined as

https://doi.org/10.1021/jasms.1c00144
J. Am. Soc. Mass Spectrom. 2021, 32, 2621−2630

$$R_p = \frac{t_A}{w} \quad (5)$$

where t_A is the ion's arrival time and w is the temporal peak width-at-half-maximum. Since mobility peak broadening can also be a sign of inadequate two-peak resolution, control of ion population homogeneity, and by extension resolving power, limits the uncertainty associated with the measured arrival times.[33,40] Lastly, protein ion clustering, which has been observed at reduced electric field strengths,[41] is often ignored. Due to these sources of potential error, the IM community recently published guidelines emphasizing the need to report propagated errors for both mobility and ^{DT}CCS values measured by DT-IM.[18]

Traveling-wave ion mobility spectrometers (TWIMS) use nonuniform electric fields to propel ions through the drift cell, which allows users to change parameters, such as wave height and velocity, to optimize ion separation. By doing this, instruments that use traveling-wave (TWAVE) technology are not limited by drift cell length. However, TWIMS requires calibration to determine CCS values (^{TW}CCS) for proteins and protein complexes because the electric field is not constant.[42−45] In DT-IM, t_d is directly related to the opposing forces that cause ion acceleration in the potential field and deceleration due to collisions with the buffer gas. However, for TWIMS, t_d is affected by the traveling wave parameters, and because the potential field is not constant, K cannot be measured directly.[18] Therefore, current methods calibrate arrival times of denatured or native-like proteins measured in TWIMS against literature ^{DT}CCS values. During calibration, uncertainty is introduced to the measurement from calibration and uncertainties in the reported ^{DT}CCS values for protein standards. These uncertainties are in addition to the random error associated with replicate measurements. Together, these uncertainties are expected to be between ±5% to 8% of the calculated ^{TW}CCS.[43] However, in the current literature, it is common to report an average ^{TW}CCS with only the associated standard deviation[46−48] or partial error propagation,[49] accounting for a small portion of the experimental error. Figure 1 shows sources of uncertainty for both DT-IM and TWIMS.

Herein, we define partial error propagation as the sum of the squares of the standard deviation of replicate CCS measurements, the error associated with the calibration curve, and the uncertainty of the calibrant CCS values. Though this method has been used to report uncertainty with TWIMS calibrations,[50] it fails to consider how the uncertainty propagates through the multiple equations used to calculate the final ^{TW}CCS. When a value, which has an uncertainty associated with it, is used to calculate another value, the initial uncertainty can increase significantly, depending on the applied mathematical function. The partial propagation method fails to consider how the uncertainty compounds with each mathematical calculation. Because of this, we hypothesize that the method of partial error propagation underestimates the uncertainty of the final ^{TW}CCS value.

We hypothesize that limiting reported uncertainty to the standard deviation or partial error propagation inaccurately describes the measurement precision. Because native MS and IM are regularly used for structural biology analyses across different platforms and often compared to computationally determined CCS values,[51−53] it is necessary to include the uncertainty associated with these measurements to allow for robust, thorough comparison. Furthermore, for proteins and complexes with unknown structures, reporting these uncertainties will enable comparison to structures that may be reported in the future. Here, we detail how to propagate error associated with a commonly used TWIMS calibration method. Further, we show that error propagation increases agreement, within experimental error, between the measured ^{TW}CCS values and literature ^{DT}CCS values for four folded proteins.

EXPERIMENTAL SECTION

Materials. Lyophilized myoglobin from equine skeletal muscle (95−100% purity), ubiquitin from bovine erythrocytes (≥98% purity), and cytochrome *c* from equine heart (≥95% purity) were from Sigma-Aldrich (St. Louis, MO). Methanol was from Thermo Fisher (Thermo Fisher Scientific Inc., Waltham, MA). All other materials were from VWR International (Radnor, PA). Nanopure water was acquired from a Purelab Flex 3 purification system (Elga, Veolia Environment S.A., Paris, France).

Sample Preparation. For native-like samples, lyophilized proteins were dissolved in 200 mM ammonium acetate, pH ∼ 7.0, and desalted using micro Bio-spin P-6 gel columns (Bio-Rad Laboratories, Mississauga, ON). The final concentration of each protein was 10 μM. After preparation, native-like samples were kept on ice when not in use. For denatured samples, lyophilized proteins were dissolved in nanopure water and diluted to final protein concentrations of 10 μM in 50:48:2 (v/v/v) methanol/water/formic acid. All samples were prepared fresh daily.

MS Analysis. Samples were loaded into pulled capillaries before being introduced to the instrument. Glass capillaries (Sutter Instrument Company, Novato, CA) were pulled to an inner diameter of ∼10 μm using a P-1000 micropipette puller (Sutter Instrument Company). The inner diameter of the tips was measured using a Hitachi TSM3030 Plus tabletop scanning electron microscope (Hitachi High-Tech, Tokyo, Japan). The tips were mounted to a tip holder and aligned to the source using an XYZ stage. A platinum wire was inserted into the liquid to apply potential for electrospray. The platinum wire was cleaned with methanol followed by nanopure water between each replicate as well as between protein samples.

A Waters Synapt G2-S High Definition MS (Waters Corporation, Millford, MA) with N_2 gas (>99.999%) in the IM cell, He gas (>99.999%) in the helium cell, and Ar gas (>99.999%) in the trap and transfer cells, was used. In the G2-S, He from the helium cell can leak into the IM cell, resulting in an unintended mixture of drift gases (Figure 1). This adds uncertainty to CCS calibrations (see below, eq 10), which assumes the use of a homogeneous drift gas.

Voltage was applied to the tip holder starting at 0.20 kV and increased by 0.20 kV until a Taylor cone was formed and signal was stable. The operating potential was dependent on the spray solvent and ranged from 1.10 kV to 1.60 kV for native-like samples (folded ubiquitin, cytochrome *c*, holo-myoglobin, and apo-myoglobin) and 0.80−1.40 kV for denatured calibrants (ubiquitin, cytochrome *c*, and apo-myoglobin). IM wave velocity and height were 250 m/s and 20 V, respectively. Transfer wave velocity and height were 200 m/s and 8 V, respectively. Additional MS and IM parameters can be found in Table S1. Mass spectra were generated by signal averaging over a 10- to 20 min acquisition. Arrival times were analyzed using MassLynx Version 4.2 (Waters Corp.).

https://doi.org/10.1021/jasms.1c00144
J. Am. Soc. Mass Spectrom. 2021, 32, 2621−2630

The sampling frequency of the instrument is another source of error that should be considered (Figure 1). While an analyte's arrival time is the time it takes for it to traverse the IM cell, the analyte must also travel through a transfer cell and through the mass analyzer before detection. Therefore, the time resolution of IM experiments is limited by the TOF-MS sampling frequency. Our instrument uses a TOF analyzer and has a time resolution that corresponds to $\frac{1}{\text{TOF-MS freq}}$. For a TOF-MS frequency of 10 kHz, this corresponds to uncertainties of 2% and 1% for arrival times of 5 ms and 10 ms, respectively.

Calibration using Denatured Calibrants. Calibration followed the protocol by Ruotolo et al.,[43] herein referred to as the Robinson method. Using a TWIMS instrument with N_2 buffer gas, we measured and extracted the arrival times for numerous charge states of denatured calibrants in six replicate trials ($t_{A,1}$ through $t_{A,6}$) (see Table S2). Denatured calibrants were chosen for these experiments due to their extensive characterization and wide range of reported CCS values (1525−3815 Å^2).[54,55] We used two sets of reported ^{DT}CCS values for our calibration curves: one measured in N_2[56] (see Table S3) and the other measured in He[55−57] (see Table S4). We made a third calibration curve using native-like calibrants whose ^{DT}CCS values were reported in He[56] (see Table S5). We did not observe significant differences between the $^{TW}CCS_{N2\rightarrow He}$ values calculated from the calibration curves using either denatured or native-like calibrants (see Figures S1 and S2 and Table S6).

To calibrate, we determined a corrected arrival time (t'_A) for each charge state of all calibrants, where C is the instrument-dependent enhanced duty cycle (EDC) delay coefficient and m/z is the mass-to-charge ratio for the calibrant at a particular charge state.[43]

$$t'_A = t_A - \left[\frac{C\sqrt{\frac{m}{z}}}{1000}\right] \tag{6}$$

We then calculated corrected CCS values (Ω')[43] based on either the $^{DT}CCS_{N2}$[56] or $^{DT}CCS_{He}$[55−57] values reported in literature (Ω), the protein charge state (z), and the reduced mass of the protein and IM drift gas (μ).

$$\Omega' = \frac{\Omega}{z\sqrt{\frac{1}{\mu}}} \tag{7}$$

Next, we generated a plot of $\ln t'_A$ against $\ln\Omega'$ and fit the plot to a linear relationship where X is the slope and $\ln A$ is the y-intercept (see Figures S1 and S2).

$$\ln\Omega' = X\ln t'_A + \ln A \tag{8}$$

Calculation of ^{TW}CCS for Native-like Proteins. We determined CCS values ($^{TW}CCS_{N2}$ and $^{TW}CCS_{N2\rightarrow He}$) for a set of folded, native-like proteins and propagated the associated uncertainty using the linear-calibration method described above.[43] We measured and extracted the arrival times for numerous charge states of our folded, native-like proteins in six replicate trials ($t_{A,1}$ through $t_{A,6}$) (see Figures S3 and S4 and Table S7). We determined the arrival time (t_A), then used eqs 6 and 8 to calculate t'_A and $\ln\Omega'$, respectively.

To calculate ^{TW}CCS for folded, native-like proteins, the Robinson method uses eq 9, which contains a power law relationship, where A and X are determined from the calibration curve.

$$\Omega = At'^{x}_{A} z\sqrt{\frac{1}{\mu}} \tag{9}$$

For the purpose of error propagation (see below), we rearranged eq 9 and utilized the identity defined in eq 8, resulting in eq 10.

$$\Omega = \exp(\ln\Omega')z\sqrt{\frac{1}{\mu}} \tag{10}$$

We then compared measured ^{TW}CCS values for the folded proteins to literature values ($^{DT}CCS_{N2}$ and $^{DT}CCS_{He}$).[55−57]

Uncertainty Calculations for Native-like Proteins. To calculate the standard deviation of replicate ^{TW}CCS values for the folded proteins, the arrival times from our six replicates ($t_{A,1}$ through $t_{A,6}$) were used to calculate six ^{TW}CCS values ($^{TW}CCS_1$ through $^{TW}CCS_6$) using eqs 6−10. An average CCS and standard deviation were then determined, $^{TW}(CCS_{avg} \pm CCS_{std})$.

In comparison, to propagate error through the calibration, we calculated an average, observed arrival time and standard deviation ($t_{A,avg} \pm t_{A,std}$) from the six replicate trials of native-like proteins. Using $t_{A,avg}$, we calculated ^{TW}CCS using eqs 6−10. Then we propagated the error through each step of the calibration to determine the uncertainty, $^{TW}(CCS \pm CCS_{uncert})$.

We determined the uncertainty associated with the arrival time correction ($e_{t'_A}$). For subtraction of a constant (see eq 6), the constant is omitted during error propagation;[58] thus, the absolute error for t'_A is the same as $t_{A,std}$.

$$e_{t'_A} = \sqrt{(t_{A,std})^2} \tag{11}$$

We determined the error of the natural log function ($e_{\ln t'_A}$) by dividing $e_{t'_A}$ by t'_A.[58]

$$e_{\ln t'_A} = \frac{e_{t'_A}}{t'_A} \tag{12}$$

To propagate the error associated with our calibration curve, we used the LINEST function in Excel to determine the error associated with the slope (e_x) and y-intercept ($e_{\ln A}$). The LINEST function is based on the method of least-squares, which assumes that there is no error associated with the x values. Therefore, we used all replicate arrival times to generate the calibration curves.

We then propagated the error for $X\ln t'_A$ ($e_{X\ln t'_A}$).

$$\frac{e_{X\ln t'_A}}{X\ln t'_A} = \sqrt{\left(\frac{e_x}{x}\right)^2 + \left(\frac{e_{\ln t'_A}}{\ln t'_A}\right)^2} \tag{13}$$

Based on eq 8, we found the error for $\ln\Omega'$ ($e_{\ln\Omega',a}$) using eq 14.

$$e_{\ln\Omega',a} = \sqrt{e^2_{X\ln t'_A} + e^2_{\ln A}} \tag{14}$$

Two denatured calibrant proteins, ubiquitin[57] and cytochrome c,[59] have reported $^{DT}CCS_{He}$ uncertainties of approximately 1% for multiple charge states. Therefore, past work has made the assumption that other protein calibrants have ^{DT}CCS values with a 1% uncertainty.[43,50] We assumed a 1% uncertainty for the $^{DT}CCS_{He}$ values for all denatured and

https://doi.org/10.1021/jasms.1c00144
J. Am. Soc. Mass Spectrom. 2021, 32, 2621−2630

native-like calibrant proteins at all charge states. The denatured calibrants measured in N_2 had reported standard deviations for each charge state for all the proteins analyzed here. These uncertainties (Ω_{stdev}) in calibrant ^{DT}CCS add uncertainty to the $\ln\Omega'$ values used to generate the calibration curve. To account for these uncertainties, we first determined the error for Ω' for each calibrant charge state ($e_{\Omega',calibn}$)) by dividing the reported uncertainty, (Ω_{stdev}) by the product of z and $\left(\frac{1}{\mu}\right)^{0.5}$ (see eq 7).

$$e_{\Omega',calibn} = \frac{\Omega_{stdev}}{z\left(\frac{1}{\mu}\right)^{0.5}} \quad (15)$$

We determined the error associated with the natural log function ($e_{ln\Omega',calibn}$) for each calibrant by dividing $e_{\Omega',calibn}$ by Ω'.

$$e_{ln\Omega',calibn} = \frac{e_{\Omega',calibn}}{\Omega',calibn} \quad (16)$$

We averaged the $e_{ln\Omega',calibn}$ values.

$$e_{ln\Omega',calib} = \frac{\sum e_{ln\Omega',calibn}}{n} \quad (17)$$

The LINEST function in Excel calculates the root-mean-square error of the calibration curve (cal_{rmse}) using eq 18, where $(y - (b - mx_i))^2$ describes the residuals, or the vertical deviation of each point from the strait line, and n is the number of data points.

$$cal_{rmse} = \sqrt{\frac{\sum (y - (b - mx_i)^2}{n - 2}} \quad (18)$$

Then, we combined $e_{ln\Omega',calib}$, cal_{rsme}, and $e_{ln\Omega',a}$ from the calibration curve (eq 14).

$$e_{ln\Omega'} = \sqrt{(e_{ln\Omega',calib})^2 + (cal_{rmse})^2 + (e_{ln\Omega',a})^2} \quad (19)$$

Finally, we derived eq 10 to prevent propagating error through a power function where the power has error associated with it. To determine the uncertainty of ^{TW}CCS ($^{TW}CCS_{uncert}$), the value of Ω (eq 10) was multiplied by the error of $\ln\Omega'$.

$$CCS_{uncert} = e_{ln\Omega'}(\exp(\ln\Omega'))z\left(\frac{1}{\mu}\right)^{0.5} \quad (20)$$

For the partial error propagation calculations (CCS_{part}), we followed eq 21, where CCS_{std} is the standard deviation of the calculated CCS values, cal_{rsme} is the root-mean-square error of the calibration curve, and $e_{\Omega',calib}$ is the uncertainty of the calibrant ^{DT}CCS values (assumed to be 1%).

$$CCS_{part} = \sqrt{CCS_{std}^2 + cal_{rsme}^2 + e_{\Omega',calib}^2} \quad (21)$$

Replicates and Statistics. Six replicates were taken throughout the day on four different days for both the denatured calibrants and folded proteins. On each day we performed separate calibrations and ^{TW}CCS calculations to examine the intermediate measurement precision.

In general, F-tests and t tests, at the 95% confidence interval, were used to compare ^{TW}CCS to the McLean data. Alternatively, 95% confidence intervals were calculated from the ^{TW}CCS values to compare to the Clemmer data. However, for the 7+ ion population of cytochrome c, the calculated $^{TW}CCS_{std}$ values were zero. Therefore, we calculated 95% confidence intervals from the McLean data and compared the confidence interval to calculated $^{TW}CCS_{avg}$ values. There were three McLean $^{DT}CCS_{He}$ values with reported standard deviations of zero. For these values, we compared 95% confidence intervals calculated from the $^{TW}CCS_{avg}$ values to the $^{DT}CCS_{He}$ values reported by the McLean group.

Lastly, we plotted Venn diagrams of our data using a program developed by the Pacific Northwest National Laboratory.[60]

RESULTS AND DISCUSSION

^{TW}CCS Values Are Similar, Independent of Calculation Method. We compared $^{TW}(CCS_{avg})_{N2}$ and $^{TW}CCS_{N2}$ values calculated using either individual arrival times or an average arrival time, respectively (Table 1). The calculated $^{TW}CCS_{N2}$ values were the same for all charge states of ubiquitin using both calculation methods. Additionally, for most charge states of cytochrome c, the $^{TW}CCS_{N2}$ values were the same for both calculation methods. For one of the ion populations associated with the 7+ charge state of cytochrome c, similar $^{TW}CCS_{N2}$ values were measured (2310 Å^2 versus 2300 Å^2), but they differed due to the uncertainty and thus the number of significant figures that were reported. We observed this trend for two additional proteins (see Table S8).

Table 1. Comparison of Measured $^{TW}CCS_{N2}$ and Literature $^{DT}CCS_{N2}$ Values

z	$^{TW}(CCS_{avg} \pm CCS_{std})_{N2}$ (Å^2)	$^{TW}(CCS \pm CCS_{uncert})_{N2}$ (Å^2)	McLean $^{DT}(CCS \pm CCS_{std})_{N2}$ (Å^2)[b]
		Cytochrome c	
5+	1400 ± 20	1400 ± 60	1400 ± 10
6+	1600 ± 20*	1600 ± 70*	1480 ± 10
7+	2010 ± 20*	2010 ± 90*	2120 ± 20
7+	2310 ± 30	2300 ± 110	–[a]
8+	2120 ± 10	2120 ± 90	2110 ± 30
8+	2400 ± 20*	2400 ± 110	2440 ± 20
		Ubiquitin	
5+	1300 ± 10*	1300 ± 60*	1220 ± 20
6+	1680 ± 10*	1680 ± 70	1630 ± 10
7+	1830 ± 0*	1830 ± 80	1870 ± 10

[a]Dashes represent the absence of literature values for the specified protein charge state. *Indicates values that are statistically different than McLean literature values at the 95% confidence interval. [b]See May et al.[56]

We also compared $^{TW}(CCS_{avg})_{N2\rightarrow He}$ and $^{TW}CCS_{N2\rightarrow He}$ following calibration using $^{DT}CCS_{He}$ (Table 2). For most of our samples, the $^{TW}CCS_{N2\rightarrow He}$ values were the same for both calculation methods. This can be seen for the ion populations of cytochrome c at the 5+, 6+, and for one set of the 7+ and 8+ charge states (1700 and 1750 Å^2, respectively). This was also observed for all charge states of ubiquitin. For the remaining conformers of cytochrome c (7+ and 8+ charge states), the $^{TW}(CCS_{avg})_{N2\rightarrow He}$ and $^{TW}CCS_{N2\rightarrow He}$ values are similar, though the magnitude of the uncertainty alters the significant figures that we report in Table 2. This trend was also observed for two additional proteins (see Tables S9 and S10).

Similar ^{TW}CCS values result when either individual arrival times or an average arrival time are used for calculation of

https://doi.org/10.1021/jasms.1c00144
J. Am. Soc. Mass Spectrom. 2021, 32, 2621−2630

Table 2. Comparison of Measured $^{TW}CCS_{N2\rightarrow He}$ and Literature $^{DT}CCS_{He}$ Values

z	$^{TW}(CCS_{avg} \pm CCS_{std})_{N2\rightarrow He}$ (Å^2)	$^{TW}(CCS \pm CCS_{uncert})_{N2\rightarrow He}$ (Å^2)	McLean $^{DT}(CCS \pm CCS_{std})_{He}$ (Å^2)[a]	Clemmer $^{DT}CCS_{He}$ (Å^2)[b,c]	% difference (McLean vs Clemmer)
			Cytochrome *c*		
5+	1170 ± 20*#	1170 ± 60*	1100 ± 10	1196	8.27
6+	1320 ± 10*#	1320 ± 60*#	1400 ± 10	1393	0.501
7+	1700 ± 20#	1700 ± 80#	1690 ± 30	1785	5.47
7+	2030 ± 30*	2000 ± 100*	1830 ± 30	2007	9.23
8+	1750 ± 10*#	1750 ± 80	1800 ± 20	1702	5.60
8+	2050 ± 30	2100 ± 100	2050 ± 0	2061	0.536
			Ubiquitin		
5+	1070 ± 10#	1070 ± 50	1050 ± 20	1027	2.21
6+	1410 ± 10*#	1410 ± 70#	1370 ± 20	1525	10.7
7+	1510 ± 0*#	1510 ± 70	1550 ± 10	1580	1.92

*Indicates values that are statistically different than McLean literature values at the 95% confidence interval. #Indicates values that are statistically different than the Clemmer literature values at the 95% confidence interval. [a]See May et al.[56] [b]See Valentine et al.[57] [c]See Shelimov et al.[55]

^{TW}CCS. This is expected since the same data and equations were used for both analyses. Similar results were seen on all days of analysis (see Tables S11 and S12).

^{DT}CCS Literature Values Vary Based on Drift Gas and Instrumentation. Before we compared our calculated ^{TW}CCS values to literature values, we first compared literature ^{DT}CCS values to each other. We used two databases for comparison: the Clemmer database[55,57] and the McLean compendium.[56] The values reported by the Clemmer group utilized a drift tube containing He while the values in the McLean compendium were determined using drift tubes containing either He or N_2 as the drift gas.[56] Table 1 shows $^{DT}CCS_{N2}$ values from the McLean group while Table 2 shows $^{DT}CCS_{He}$ values from both groups. Additional $^{DT}CCS_{N2}$ and $^{DT}CCS_{He}$ values can be found in Tables S8−S10.

The contrast in $^{DT}CCS_{He}$ and $^{DT}CCS_{N2}$ values can be attributed to differences of analyte mobility in the different drift gases. Interactions between an analyte and He are comparable to collisions with a hard sphere, while long-range interactions between the same analyte and N_2 are more readily achieved due to the polarizability of N_2.[16,61] To put it simply, when interacting with the hard-sphere-like He, the analyte will either hit or miss the drift gas. Conversely, the same analyte will experience long-range interactions when interacting with N_2.[61] These long-range interactions contribute to the larger observed K, and by extension CCS, values measured in N_2.[56,62−64] In addition, as an analyte's charge increases, the analyte may take an extended form to minimize Coulombic repulsion. It has been shown that when using a polarizable gas, such as N_2, the magnitude of the CCS scales with the analyte charge state due to this change in size.[32] Peptides, which have lower charge states, tend to have CCS values that can be correlated across different drift gases. However, proteins, which have higher charge states, and thus different extended forms, interact with each drift gas differently, resulting in a more diverse range of reported CCS values.[32,65] Therefore, it is uncommon to compare $^{DT}CCS_{He}$ and $^{DT}CCS_{N2}$ values for proteins.

Additionally, the ion population that is measured during IM may be affected by processes that unfold the protein or alter its structure before or during IM. It has been suggested that protein ^{DT}CCS values determined using a drift tube containing He reflect some degree of unfolding associated with collisional heating of the protein ions due to the higher pressure required for operation.[56] This results in fewer conformations and fewer $^{DT}CCS_{He}$ values compared to the number of conformations measured when using N_2 as a drift gas.[32,56]

Looking at Table 2, we see differences in the two sets of literature $^{DT}CCS_{He}$ values. The percent difference was calculated using eq 22, where $CCS_{He,Clemmer}$ represents $^{DT}CCS_{He}$ values determined by the Clemmer group and $CCS_{He,McLean}$ represents $^{DT}CCS_{He}$ values determined by the McLean group.

$$\%\text{diff} = 100 \times \left(\frac{|CCS_{He,Clemmer} - CCS_{He,McLean}|}{\sum (CCS_{He})/2} \right) \quad (22)$$

Smaller percent differences illustrate more consistent values. We see a wide range of percent difference between the two literature sets, with the lowest being 0.501% (indicating highly consistent $^{DT}CCS_{He}$ values) and the highest being 10.7% (indicating different $^{DT}CCS_{He}$ values).

These differences are likely due to (1) several of the assumptions discussed in the introduction and (2) the different platforms that were used. An ion's gas-phase structure can change due to differences in sample preparation and source conditions.[18] Thus, when comparing CCS values determined using different platforms, different gas-phase ion conformations may result. Additionally, differences in the temperature and pressures within the drift cells could affect the reported $^{DT}CCS_{He}$ values. As described above, the conformers present during IM are dependent on ionization and ion heating. Differences in the instruments may have resulted in different levels of protein unfolding during ionization and as a result of ion heating. Therefore, instrument and sample preparation differences likely contribute to why the McLean and Clemmer $^{DT}CCS_{He}$ values are statistically different for most protein conformations.

$^{TW}CCS_{uncert}$ Are Less Precise than $^{TW}CCS_{std}$. We compared the magnitude of the uncertainty for $^{TW}(CCS_{std})_{N2\rightarrow He}$ versus $^{TW}(CCS_{uncert})_{N2\rightarrow He}$. Table 2 shows that $^{TW}(CCS_{uncert})_{N2\rightarrow He}$ is consistently higher than $^{TW}(CCS_{std})_{N2\rightarrow He}$ for all charge states of each protein. The calculated $^{TW}CCS_{N2\rightarrow He}$ and associated uncertainties for two additional proteins are presented in Table S9. This trend can also be seen for $^{TW}(CCS_{std})_{N2}$ and $^{TW}(CCS_{uncert})_{N2}$ (see Table 1 and Table S8). When calculating $^{TW}(CCS_{std})_{N2\rightarrow He}$, the uncertainty mostly relates to the variability associated with replicate measurements. For all four proteins, the average relative standard deviation (RSD) was 1% of the calculated

https://doi.org/10.1021/jasms.1c00144
J. Am. Soc. Mass Spectrom. 2021, 32, 2621−2630

$^{TW}(CCS_{avg})_{N2\rightarrow He}$ value. For comparison, we calculated uncertainty based on partial error propagation (eq 21)[50] and concluded that the resulting uncertainty was less than 2% RSD of the final $^{TW}(CCS_{avg})_{N2\rightarrow He}$ values. Both values are less than the anticipated 5% to 8% error suggested by Ruotolo et al.[43] following calibration. In comparison, when we calculate $^{TW}(CCS_{uncert})_{N2\rightarrow He}$, we include the uncertainties associated with calibration and the calibrant standards. Our propagated error values are consistently between 4% and 6% RSD of the calculated $^{TW}CCS_{N2\rightarrow He}$ values, with the average RSD for all four proteins being 5%.

Propagating Error Improves Agreement, within Experimental Error, between Calculated ^{TW}CCS Values and Literature ^{DT}CCS Values. In addition to calculated $^{TW}CCS_{N2}$ values, Table 1 shows $^{DT}CCS_{N2}$ values from the McLean group. When comparing the experimental values to literature $^{DT}CCS_{N2}$ values, we see that there are several instances where $^{TW}(CCS_{avg} \pm CCS_{std})_{N2}$ are statistically different from the literature values but $^{TW}(CCS \pm CCS_{uncert})_{N2}$ are within the experimental error of the literature values. We see this with the ion population of the 6+ charge state of ubiquitin where the $^{TW}(CCS_{avg} \pm CCS_{std})_{N2}$ value of (1680 ± 10) Å^2 is statistically different from the literature $^{DT}CCS_{N2}$ value of (1630 ± 10) Å^2, but the $^{TW}(CCS \pm CCS_{uncert})_{N2}$ value of (1680 ± 70) Å^2 is within the experimental error of the literature value. This can also be seen for ion populations associated with the 7+ charge state of ubiquitin and one conformer of the 8+ charge state of cytochrome *c*. We see a similar trend for two other proteins (see Table S8). When considering all four proteins, we see that 14% of the $^{TW}(CCS_{avg} \pm CCS_{std})_{N2}$ values agree, within experimental error, to McLean literature $^{DT}CCS_{N2}$ values. However, 50% of $^{TW}(CCS \pm CCS_{uncert})_{N2}$ values are within the error of the McLean literature values.

Table 2 also shows literature values for two native-like proteins measured using DT-IM in He. When comparing the experimental $^{TW}(CCS \pm CCS_{uncert})_{N2\rightarrow He}$ and literature $^{DT}CCS_{He}$ values, two different observations were made. First, for some of the data, the values reported by the Clemmer and McLean groups generated a range that encompassed the average, experimental $^{TW}CCS_{N2\rightarrow He}$ value. This was observed for the ion population of the 5+ charge state of cytochrome *c*, where the range of 1196 Å^2 (Clemmer) to 1100 Å^2 (McLean) encompass the average, calculated $^{TW}CCS_{N2\rightarrow He}$ of 1170 Å^2. Second, some of the experimental $^{TW}CCS_{N2\rightarrow He}$ values were similar to either the McLean or Clemmer literature values, but not both. This is seen for one of the ion populations associated with the 7+ charge state of cytochrome *c*, where the $^{TW}CCS_{N2\rightarrow He}$ of (2000 ± 100) Å^2 aligns with the $^{DT}CCS_{He}$ reported by the Clemmer lab (2007 Å^2) but was statistically different from that reported in the McLean compendium (1830 ± 30 Å^2).

It was more common for the calculated $^{TW}(CCS \pm CCS_{uncert})_{N2\rightarrow He}$ values to agree, within error, with one set of $^{DT}CCS_{He}$ literature values compared to agreeing with both sets or neither set of literature values. Alternatively, the $^{TW}(CCS_{avg} \pm CCS_{std})_{N2\rightarrow He}$ values differed from both sets of literature values more than they agreed with one or both sets of literature values (Figure 2).

For cytochrome *c*, 33% of the calculated $^{TW}(CCS_{avg} \pm CCS_{std})_{N2\rightarrow He}$ values agreed, within error, with the McLean $^{DT}CCS_{He}$ literature values (Table 2). We see an increase to 50% agreement when incorporating error propagation and comparing $^{TW}(CCS \pm CCS_{uncert})_{N2\rightarrow He}$ to the McLean $^{DT}CCS_{He}$ literature values. This trend was also observed when comparing experimental values with and without error propagation to the reported literature values for ubiquitin, apomyoglobin, and holo-myoglobin (see Table S9). When considering all four proteins, 27% of the $^{TW}(CCS_{avg} \pm CCS_{std})_{N2\rightarrow He}$ values agree, within error, to McLean $^{DT}CCS_{He}$ literature values. This agreement increases to 67% when comparing $^{TW}(CCS \pm CCS_{uncert})_{N2\rightarrow He}$ to $^{DT}CCS_{He}$ literature values.

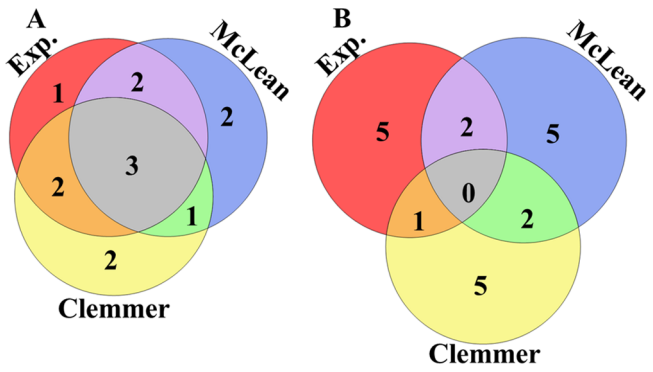

Figure 2. Venn diagrams illustrating agreement between literature ^{DT}CCS values and experimental (A) $^{TW}(CCS \pm CCS_{uncert})_{N2\rightarrow He}$ or (B) $^{TW}(CCS_{avg} \pm CCS_{std})_{N2\rightarrow He}$ values. McLean $^{DT}CCS_{He}$ are in blue, Clemmer $^{DT}CCS_{He}$ are in yellow, and experimental (Exp.) $^{TW}CCS_{N2\rightarrow He}$ are in red. Comparisons include ion-neutral CCS from eight detected charge states of cytochrome *c*, ubiquitin, and apomyoglobin, all of which had standard deviations not equal to zero. For (B), the McLean $^{DT}CCS_{He}$ for the 5+ charge state of ubiquitin agreed with the experimental $^{TW}CCS_{N2\rightarrow He}$ and Clemmer $^{DT}CCS_{He}$, but the experimental $^{TW}CCS_{N2\rightarrow He}$ did not agree with the Clemmer $^{DT}CCS_{He}$. Venn diagrams highlight the improved agreement between $^{TW}CCS_{N2\rightarrow He}$ and $^{DT}CCS_{He}$ values when error is propagated through the calibration.

Similarly, we see that for cytochrome *c*, 33% of calculated $^{TW}(CCS_{avg} \pm CCS_{std})_{N2\rightarrow He}$ values agree, within error, to the Clemmer $^{DT}CCS_{He}$ literature values (Table 2). We see an increase to 67% agreement between $^{TW}(CCS \pm CCS_{uncert})_{N2\rightarrow He}$ and Clemmer $^{DT}CCS_{He}$ literature values when incorporating error propagation to our analysis. Furthermore, we observe only 15% agreement between experimental $^{TW}(CCS_{avg} \pm CCS_{std})_{N2\rightarrow He}$ values for all four proteins and Clemmer $^{DT}CCS_{He}$ literature values (see Table S10). This agreement increases to 69% when comparing experimental $^{TW}(CCS \pm CCS_{uncert})_{N2\rightarrow He}$ and $^{DT}CCS_{He}$ literature values. Thus, by incorporating error propagation through our measurements, we were able to measure $^{TW}CCS_{N2\rightarrow He}$ values that had improved accordance with two different DT-IM platforms.

In this paper, we calculated both $^{TW}CCS_{N2}$ and $^{TW}CCS_{N2\rightarrow He}$ values using an IM cell with N_2 and calibrant ^{DT}CCS values measured with either N_2 or He. However, in the Synapt G2-S, the TWIMS cell may contain a mixture of both He and N_2 in the IM cell due to leakage from the He cell. This could increase the uncertainty of the calculated ^{TW}CCS values. If the exact molar fractions of the two gases are known, then they could be accounted for using Blanc's law. A recent publication suggests that, with knowledge of mobilities in neat gases, Blanc's law can be applied retrospectively.[28] However, in

https://doi.org/10.1021/jasms.1c00144
J. Am. Soc. Mass Spectrom. 2021, 32, 2621−2630

the Synapt G2-S, we do not know the exact molar ratio of the two gases. Though we anticipate that the gas mixture adds uncertainty, Gabelica et al. suggests that the uncertainty may be minimal.[18] This may explain why we see reasonable correlation between our ^{TW}CCS values and the literature values, whether we compare $^{TW}CCS_{N2}$ to $^{DT}CCS_{N2}$ or $^{TW}CCS_{N2\rightarrow He}$ to $^{DT}CCS_{He}$.

CONCLUSIONS

IM allows for the determination of an ion's gas-phase mobility by measuring the momentum transfers that occur as ions move through a drift cell containing an inert buffer gas. The average of the momentum transfers is reported as a momentum transfer cross section (CCS), which is partially related to ion structures. TWIMS is one such IM technique that has the capability to discern structural differences between gas-phase ion populations. However, TWIMS inadvertently introduces error into structural comparisons due to the need for calibration. While it is not currently common to consider all error contributions, we have shown that error propagation through the TWIMS calibration significantly increases the agreement, within error, between calculated ^{TW}CCS values and literature ^{DT}CCS values, compared to reporting only the standard deviation of replicate measurements. Additionally, the propagated error values fall within the predicted ±5% to 8% range defined by Ruotolo et al.[43]

Herein, error propagation was applied to the calibration of known ^{DT}CCS values versus the arrival times of denatured calibrants. However, the utility of propagating error through the calibration is relevant as the IM community moves toward using native-like, folded protein calibrants[16,66,67] or considers calibrating ion mobility (K) rather than CCS values, as has been recently suggested for DT-IM.[18]

Additionally, beyond the Waters Synapt platform, other TWIMS devices are becoming commercially available. We expect to see an increase in agreement between experimental ^{TW}CCS and literature ^{DT}CCS values when using error propagation for any of these TWIMS instruments that require calibration, such as in structures for lossless ion manipulations (SLIM)[68−70] or cyclic IM-MS.[71] This method of error propagation can be formatted to fit any type of mathematical equation, thus allowing for incorporation of all uncertainties that would arise from experimentation and data analysis. Regardless of what calibrants or calibration is used, regular use of error propagation in calibration of any TWIMS device will further legitimize the use of native IM-MS for analyses related to structural biology. Furthermore, wide use of error propagation will allow for more robust comparison of ion-neutral CCS values determined by various groups using different platforms.

We cannot know a protein's "true" gas-phase mobility *a priori* as it is a property of the ion and neutral-species and is thus dependent on experimental conditions.[17,18] Therefore, the calibration required for TWIMS allows users to compare, not validate, experimental data to other platforms and to computationally determined CCS values. In this Critical Insight, we describe multiple assumptions and uncertainties that affect CCS values, whether they are derived from mobility measurements in DT-IM or calculated following calibration of TWIMS. We put forth a challenge to the IM community to reconsider how TWIMS calibration, and its associated uncertainty, are regarded and used. Herein, we present a method that propagates error through ^{TW}CCS calibrations to provide a more robust picture of measurement uncertainty.

ASSOCIATED CONTENT

Supporting Information

The Supporting Information is available free of charge at https://pubs.acs.org/doi/10.1021/jasms.1c00144.

Additional instrumental parameters, selected m/z ranges with corresponding arrival times and peak widths for all samples, calibration curve data, heat maps, and tables comparing experimental and literature CCS values for all four proteins (PDF)

AUTHOR INFORMATION

Corresponding Author

Elyssia S. Gallagher − *Department of Chemistry and Biochemistry, Baylor University, Waco, Texas 76798, United States;* orcid.org/0000-0002-5411-7285; Email: Elyssia_Gallagher@baylor.edu

Authors

Alexis N. Edwards − *Department of Chemistry and Biochemistry, Baylor University, Waco, Texas 76798, United States*

Hien M. Tran − *Department of Chemistry and Biochemistry, Baylor University, Waco, Texas 76798, United States*

Complete contact information is available at: https://pubs.acs.org/10.1021/jasms.1c00144

Notes

The authors declare no competing financial interest.

ACKNOWLEDGMENTS

This work was supported by the Welch Foundation (AA-1899) and the National Science Foundation (CHE-1945078). The authors acknowledge the Baylor University Mass Spectrometry Center as well and the Center for Microscopy and Imaging. The authors thank Dr. David Russell and his group for training funded by P41 "Resource in Native MS-Guided Structural Biology" P41GM128577.

REFERENCES

(1) Nguyen, G. T. H.; Tran, T. N.; Podgorski, M. N.; Bell, S. G.; Supuran, C. T.; Donald, W. A. Nanoscale Ion Emitters in Native Mass Spectrometry for Measuring Ligand-Protein Binding Affinities. *ACS Cent. Sci.* **2019**, *5* (2), 308−318.

(2) Ahdash, Z.; Lau, A. M.; Martens, C.; Politis, A. Analyzing Protein Architectures and Protein-Ligand Complexes by Integrative Structural Mass Spectrometry. *J. Visualized Exp.* **2018**, No. 140, 57966.

(3) Saikusa, K.; Kato, D.; Nagadoi, A.; Kurumizaka, H.; Akashi, S. Native Mass Spectrometry of Protein and DNA Complexes Prepared in Nonvolatile Buffers. *J. Am. Soc. Mass Spectrom.* **2020**, *31* (3), 711−718.

(4) Nguyen, G. T. H.; Leung, W. Y.; Tran, T. N.; Wang, H.; Murray, V.; Donald, W. A. Mechanism for the Binding of Netropsin to Hairpin DNA Revealed Using Nanoscale Ion Emitters in Native Mass Spectrometry. *Anal. Chem.* **2020**, *92* (1), 1130−1137.

(5) Snijder, J.; van de Waterbeemd, M.; Damoc, E.; Denisov, E.; Grinfeld, D.; Bennett, A.; Agbandje-McKenna, M.; Makarov, A.; Heck, A. J. Defining the stoichiometry and cargo load of viral and bacterial nanoparticles by Orbitrap mass spectrometry. *J. Am. Chem. Soc.* **2014**, *136* (20), 7295−9.

(6) Frick, M.; Schmidt, C. Mass spectrometry-A versatile tool for characterising the lipid environment of membrane protein assemblies. *Chem. Phys. Lipids* **2019**, *221*, 145−157.
(7) Hellwig, N.; Peetz, O.; Ahdash, Z.; Tascon, I.; Booth, P. J.; Mikusevic, V.; Diskowski, M.; Politis, A.; Hellmich, Y.; Hanelt, I.; Reading, E.; Morgner, N. Native mass spectrometry goes more native: investigation of membrane protein complexes directly from SMALPs. *Chem. Commun. (Cambridge, U. K.)* **2018**, *54* (97), 13702−13705.
(8) Cubrilovic, D.; Barylyuk, K.; Hofmann, D.; Walczak, M. J.; Graber, M.; Berg, T.; Wider, G.; Zenobi, R. Direct monitoring of protein-protein inhibition using nano electrospray ionization mass spectrometry. *Chemical Science* **2014**, *5* (7), 2794−2803.
(9) Vivat Hannah, V.; Atmanene, C.; Zeyer, D.; Van Dorsselaer, A.; Sanglier-Cianferani, S. Native MS: an 'ESI' way to support structure- and fragment-based drug discovery. *Future Med. Chem.* **2010**, *2* (1), 35−50.
(10) Blackwell, A. E.; Dodds, E. D.; Bandarian, V.; Wysocki, V. H. Revealing the quaternary structure of a heterogeneous noncovalent protein complex through surface-induced dissociation. *Anal. Chem.* **2011**, *83* (8), 2862−5.
(11) Norris, A.; Busch, F.; Schupfner, M.; Sterner, R.; Wysocki, V. H. Quaternary Structure of the Tryptophan Synthase alpha-Subunit Homolog BX1 from Zea mays. *J. Am. Soc. Mass Spectrom.* **2020**, *31* (2), 227−233.
(12) Moreno-Pedraza, A.; Rosas-Roman, I.; Garcia-Rojas, N. S.; Guillen-Alonso, H.; Ovando-Vazquez, C.; Diaz-Ramirez, D.; Cuevas-Contreras, J.; Vergara, F.; Marsch-Martinez, N.; Molina-Torres, J.; Winkler, R. Elucidating the Distribution of Plant Metabolites from Native Tissues with Laser Desorption Low-Temperature Plasma Mass Spectrometry Imaging. *Anal. Chem.* **2019**, *91* (4), 2734−2743.
(13) Onuchic, J. N.; Luthey-Schulten, Z.; Wolynes, P. G. Theory of protein folding: the energy landscape perspective. *Annu. Rev. Phys. Chem.* **1997**, *48*, 545−600.
(14) Bryngelson, J. D.; Onuchic, J. N.; Socci, N. D.; Wolynes, P. G. Funnels, pathways, and the energy landscape of protein folding: a synthesis. *Proteins: Struct., Funct., Genet.* **1995**, *21* (3), 167−95.
(15) Lau, A. M.; Politis, A., Integrative Mass Spectrometry−Based Approaches for Modeling Macromolecular Assemblies. In *Multiprotein Complexes: Methods and Protocols*; Poterszman, A., Ed.; Springer US: New York, 2021; pp 221−241.
(16) Gabelica, V.; Marklund, E. Fundamentals of ion mobility spectrometry. *Curr. Opin. Chem. Biol.* **2018**, *42*, 51−59.
(17) Siems, W. F.; Viehland, L. A.; Hill, H. H., Jr. Improved momentum-transfer theory for ion mobility. 1. Derivation of the fundamental equation. *Anal. Chem.* **2012**, *84* (22), 9782−91.
(18) Gabelica, V.; Shvartsburg, A. A.; Afonso, C.; Barran, P.; Benesch, J. L. P.; Bleiholder, C.; Bowers, M. T.; Bilbao, A.; Bush, M. F.; Campbell, J. L.; Campuzano, I. D. G.; Causon, T.; Clowers, B. H.; Creaser, C. S.; De Pauw, E.; Far, J.; Fernandez-Lima, F.; Fjeldsted, J. C.; Giles, K.; Groessl, M.; Hogan, C. J., Jr.; Hann, S.; Kim, H. I.; Kurulugama, R. T.; May, J. C.; McLean, J. A.; Pagel, K.; Richardson, K.; Ridgeway, M. E.; Rosu, F.; Sobott, F.; Thalassinos, K.; Valentine, S. J.; Wyttenbach, T. Recommendations for reporting ion mobility Mass Spectrometry measurements. *Mass Spectrom. Rev.* **2019**, *38* (3), 291−320.
(19) Siems, W. F.; Viehland, L. A.; Hill, H. H. Correcting the fundamental ion mobility equation for field effects. *Analyst* **2016**, *141* (23), 6396−6407.
(20) Hauck, B. C.; Siems, W. F.; Harden, C. S.; McHugh, V. M.; Hill, H. H. High Accuracy Ion Mobility Spectrometry for Instrument Calibration. *Anal. Chem.* **2018**, *90* (7), 4578−4584.
(21) Patterson, D.; Tsikata, E.; Doyle, J. M. Cooling and collisions of large gas phase molecules. *Phys. Chem. Chem. Phys.* **2010**, *12* (33), 9736−41.
(22) Mason, E. A.; Monchick, L. Heat Conductivity of Polyatomic and Polar Gases. *J. Chem. Phys.* **1962**, *36* (6), 1622.
(23) Monchick, L.; Pereira, A. N. G.; Mason, E. A. Heat Conductivity of Polyatomic and Polar Gases and Gas Mixtures. *J. Chem. Phys.* **1965**, *42* (9), 3241.
(24) Bellamy-Carter, J.; O'Grady, L.; Passmore, M.; Jenner, M.; Oldham, N. J. Decoding Protein Gas-Phase Stability with Alanine Scanning and Collision-Induced Unfolding Ion Mobility Mass Spectrometry. *Analysis & Sensing* **2021**, *1* (1), 63−69.
(25) Dixit, S. M.; Polasky, D. A.; Ruotolo, B. T. Collision induced unfolding of isolated proteins in the gas phase: past, present, and future. *Curr. Opin. Chem. Biol.* **2018**, *42*, 93−100.
(26) Freeke, J.; Bush, M. F.; Robinson, C. V.; Ruotolo, B. T. Gas-phase protein assemblies: Unfolding landscapes and preserving native-like structures using noncovalent adducts. *Chem. Phys. Lett.* **2012**, *524*, 1−9.
(27) D'Atri, V.; Porrini, M.; Rosu, F.; Gabelica, V. Linking molecular models with ion mobility experiments. Illustration with a rigid nucleic acid structure. *J. Mass Spectrom.* **2015**, *50* (5), 711−26.
(28) Naylor, C. N.; Clowers, B. H. Reevaluating the Role of Polarizability in Ion Mobility Spectrometry. *J. Am. Soc. Mass Spectrom.* **2021**, *32* (3), 618−627.
(29) Morris, C. B.; May, J. C.; Leaptrot, K. L.; McLean, J. A. Evaluating Separation Selectivity and Collision Cross Section Measurement Reproducibility in Helium, Nitrogen, Argon, and Carbon Dioxide Drift Gases for Drift Tube Ion Mobility-Mass Spectrometry. *J. Am. Soc. Mass Spectrom.* **2019**, *30* (6), 1059−1068.
(30) Larriba, C.; Hogan, C. J., Jr. Ion mobilities in diatomic gases: measurement versus prediction with non-specular scattering models. *J. Phys. Chem. A* **2013**, *117* (19), 3887−901.
(31) Larriba-Andaluz, C.; Hogan, C. J., Jr. Collision cross section calculations for polyatomic ions considering rotating diatomic/linear gas molecules. *J. Chem. Phys.* **2014**, *141* (19), 194107.
(32) Jurneczko, E.; Kalapothakis, J.; Campuzano, I. D.; Morris, M.; Barran, P. E. Effects of drift gas on collision cross sections of a protein standard in linear drift tube and traveling wave ion mobility mass spectrometry. *Anal. Chem.* **2012**, *84* (20), 8524−31.
(33) Siems, W. F.; Wu, C.; Tarver, E. E.; Hill, H. H.; Larsen, P. R.; Mcminn, D. G. Measuring the Resolving Power of Ion Mobility Spectrometers. *Anal. Chem.* **1994**, *66* (23), 4195−4201.
(34) Rokushika, S.; Hatano, H.; Baim, M. A.; Hill, H. H. Resolution Measurement for Ion Mobility Spectrometry. *Anal. Chem.* **1985**, *57* (9), 1902−1907.
(35) Watts, P.; Wilders, A. On the Resolution Obtainable in Practical Ion Mobility Systems. *Int. J. Mass Spectrom. Ion Processes* **1992**, *112* (2−3), 179−190.
(36) Asbury, G. R.; Hill, H. H. Evaluation of ultrahigh resolution ion mobility spectrometry as an analytical separation device in chromatographic terms. *J. Microcolumn Sep.* **2000**, *12* (3), 172−178.
(37) Dugourd, P.; Hudgins, R. R.; Clemmer, D. E.; Jarrold, M. F. High-resolution ion mobility measurements. *Rev. Sci. Instrum.* **1997**, *68* (2), 1122−1129.
(38) Tabrizchi, M.; Rouholahnejad, F. Pressure effects on resolution in ion mobility spectrometry. *Talanta* **2006**, *69* (1), 87−90.
(39) Crawford, C. L.; Hauck, B. C.; Tufariello, J. A.; Harden, C. S.; McHugh, V.; Siems, W. F.; Hill, H. H., Jr. Accurate and reproducible ion mobility measurements for chemical standard evaluation. *Talanta* **2012**, *101*, 161−70.
(40) Kanu, A. B.; Gribb, M. M.; Hill, H. H., Jr. Predicting optimal resolving power for ambient pressure ion mobility spectrometry. *Anal. Chem.* **2008**, *80* (17), 6610−9.
(41) Schaefer, C.; Allers, M.; Kirk, A. T.; Schlottmann, F.; Zimmermann, S. Influence of Reduced Field Strength on Product Ion Formation in High Kinetic Energy Ion Mobility Spectrometry (HiKE-IMS). *J. Am. Soc. Mass Spectrom.* **2021**, *32* (7), 1810−1820.
(42) Shvartsburg, A. A.; Smith, R. D. Fundamentals of traveling wave ion mobility spectrometry. *Anal. Chem.* **2008**, *80* (24), 9689−99.
(43) Ruotolo, B. T.; Benesch, J. L.; Sandercock, A. M.; Hyung, S. J.; Robinson, C. V. Ion mobility-mass spectrometry analysis of large protein complexes. *Nat. Protoc.* **2008**, *3* (7), 1139−52.
(44) Duez, Q.; Chirot, F.; Lienard, R.; Josse, T.; Choi, C.; Coulembier, O.; Dugourd, P.; Cornil, J.; Gerbaux, P.; De Winter, J. Polymers for Traveling Wave Ion Mobility Spectrometry Calibration. *J. Am. Soc. Mass Spectrom.* **2017**, *28* (11), 2483−2491.

https://doi.org/10.1021/jasms.1c00144
J. Am. Soc. Mass Spectrom. 2021, 32, 2621−2630

(45) Smith, D. P.; Knapman, T. W.; Campuzano, I.; Malham, R. W.; Berryman, J. T.; Radford, S. E.; Ashcroft, A. E. Deciphering drift time measurements from travelling wave ion mobility spectrometry-mass spectrometry studies. *Eur. J. Mass Spectrom.* **2009**, *15* (2), 113−30.
(46) Gadkari, V. V.; Ramirez, C. R.; Vallejo, D. D.; Kurulugama, R. T.; Fjeldsted, J. C.; Ruotolo, B. T. Enhanced Collision Induced Unfolding and Electron Capture Dissociation of Native-like Protein Ions. *Anal. Chem.* **2020**, *92* (23), 15489−15496.
(47) Hale, O. J.; Sisley, E. K.; Griffiths, R. L.; Styles, I. B.; Cooper, H. J. Native LESA TWIMS-MSI: Spatial, Conformational, and Mass Analysis of Proteins and Protein Complexes. *J. Am. Soc. Mass Spectrom.* **2020**, *31* (4), 873−879.
(48) Hernandez-Mesa, M.; D'Atri, V.; Barknowitz, G.; Fanuel, M.; Pezzatti, J.; Dreolin, N.; Ropartz, D.; Monteau, F.; Vigneau, E.; Rudaz, S.; Stead, S.; Rogniaux, H.; Guillarme, D.; Dervilly, G.; Le Bizec, B. Interlaboratory and Interplatform Study of Steroids Collision Cross Section by Traveling Wave Ion Mobility Spectrometry. *Anal. Chem.* **2020**, *92* (7), 5013−5022.
(49) Griffiths, R. L.; Sisley, E. K.; Lopez-Clavijo, A. F.; Simmonds, A. L.; Styles, I. B.; Cooper, H. J. Native mass spectrometry imaging of intact proteins and protein complexes in thin tissue sections. *Int. J. Mass Spectrom.* **2019**, *437*, 23−29.
(50) Polasky, D. A.; Dixit, S. M.; Keating, M. F.; Gadkari, V. V.; Andrews, P. C.; Ruotolo, B. T. Pervasive Charge Solvation Permeates Native-like Protein Ions and Dramatically Influences Top-down Sequencing Data. *J. Am. Chem. Soc.* **2020**, *142* (14), 6750−6760.
(51) Ewing, S. A.; Donor, M. T.; Wilson, J. W.; Prell, J. S. Collidoscope: An Improved Tool for Computing Collisional Cross-Sections with the Trajectory Method. *J. Am. Soc. Mass Spectrom.* **2017**, *28* (4), 587−596.
(52) Marklund, E. G.; Degiacomi, M. T.; Robinson, C. V.; Baldwin, A. J.; Benesch, J. L. Collision cross sections for structural proteomics. *Structure* **2015**, *23* (4), 791−9.
(53) Allison, T. M.; Barran, P.; Cianferani, S.; Degiacomi, M. T.; Gabelica, V.; Grandori, R.; Marklund, E. G.; Menneteau, T.; Migas, L. G.; Politis, A.; Sharon, M.; Sobott, F.; Thalassinos, K.; Benesch, J. L. P. Computational Strategies and Challenges for Using Native Ion Mobility Mass Spectrometry in Biophysics and Structural Biology. *Anal. Chem.* **2020**, *92* (16), 10872−10880.
(54) Valentine, S. J.; Counterman, A. E.; Clemmer, D. E. A database of 660 peptide ion cross sections: Use of intrinsic size parameters for bona fide predictions of cross sections. *J. Am. Soc. Mass Spectrom.* **1999**, *10* (11), 1188−1211.
(55) Shelimov, K. B.; Clemmer, D. E.; Hudgins, R. R.; Jarrold, M. F. Protein Structure in Vacuo: Gas-Phase Conformations of BPTI and Cytochrome c. *J. Am. Chem. Soc.* **1997**, *119* (9), 2240−2248.
(56) May, J. C.; Jurneczko, E.; Stow, S. M.; Kratochvil, I.; Kalkhof, S.; McLean, J. A. Conformational Landscapes of Ubiquitin, Cytochrome c, and Myoglobin: Uniform Field Ion Mobility Measurements in Helium and Nitrogen Drift Gas. *Int. J. Mass Spectrom.* **2018**, *427*, 79−90.
(57) Valentine, S. J.; Counterman, A. E.; Clemmer, D. E. Conformer-dependent proton-transfer reactions of ubiquitin ions. *J. Am. Soc. Mass Spectrom.* **1997**, *8* (9), 954−961.
(58) Taylor, J. R. *An introduction to error analysis*; University Science Books: Sausalito, 1997.
(59) Valentine, S. J.; Clemmer, D. E. H/D exchange levels of shape-resolved cytochrome c conformers in the gas phase. *J. Am. Chem. Soc.* **1997**, *119* (15), 3558−3566.
(60) Littlefield, K.; Monroe, M. *Venn-Diamgram-Plotter*; Pacific Northwest National Laboratory, 2020.
(61) Boschmans, J.; Jacobs, S.; Williams, J. P.; Palmer, M.; Richardson, K.; Giles, K.; Lapthorn, C.; Herrebout, W. A.; Lemiere, F.; Sobott, F. Combining density functional theory (DFT) and collision cross-section (CCS) calculations to analyze the gas-phase behaviour of small molecules and their protonation site isomers. *Analyst* **2016**, *141* (13), 4044−54.
(62) Chen, S.-H.; Russell, D. H. How Closely Related Are Conformations of Protein Ions Sampled by IM-MS to Native Solution Structures? *J. Am. Soc. Mass Spectrom.* **2015**, *26* (9), 1433−1443.
(63) Sun, Y.; Vahidi, S.; Sowole, M. A.; Konermann, L. Protein Structural Studies by Traveling Wave Ion Mobility Spectrometry: A Critical Look at Electrospray Sources and Calibration Issues. *J. Am. Soc. Mass Spectrom.* **2016**, *27* (1), 31−40.
(64) France, A. P.; Migas, L. G.; Sinclair, E.; Bellina, B.; Barran, P. E. Using Collision Cross Section Distributions to Assess the Distribution of Collision Cross Section Values. *Anal. Chem.* **2020**, *92* (6), 4340−4348.
(65) Bush, M. F.; Campuzano, I. D.; Robinson, C. V. Ion mobility mass spectrometry of peptide ions: effects of drift gas and calibration strategies. *Anal. Chem.* **2012**, *84* (16), 7124−30.
(66) Eldrid, C.; O'Connor, E.; Thalassinos, K. Concentration-dependent coulombic effects in travelling wave ion mobility spectrometry collision cross section calibration. *Rapid Commun. Mass Spectrom.* **2020**, *34* (Suppl 4), e8613.
(67) Stiving, A. Q.; Jones, B. J.; Ujma, J.; Giles, K.; Wysocki, V. H. Collision Cross Sections of Charge-Reduced Proteins and Protein Complexes: A Database for Collision Cross Section Calibration. *Anal. Chem.* **2020**, *92* (6), 4475−4483.
(68) Li, A.; Conant, C. R.; Zheng, X.; Bloodsworth, K. J.; Orton, D. J.; Garimella, S. V. B.; Attah, I. K.; Nagy, G.; Smith, R. D.; Ibrahim, Y. M. Assessing Collision Cross Section Calibration Strategies for Traveling Wave-Based Ion Mobility Separations in Structures for Lossless Ion Manipulations. *Anal. Chem.* **2020**, *92* (22), 14976−14982.
(69) Hines, K. M.; Ross, D. H.; Davidson, K. L.; Bush, M. F.; Xu, L. Large-Scale Structural Characterization of Drug and Drug-Like Compounds by High-Throughput Ion Mobility-Mass Spectrometry. *Anal. Chem.* **2017**, *89* (17), 9023−9030.
(70) May, J. C.; Leaptrot, K. L.; Rose, B. S.; Moser, K. L. W.; Deng, L.; Maxon, L.; DeBord, D.; McLean, J. A. Resolving Power and Collision Cross Section Measurement Accuracy of a Prototype High-Resolution Ion Mobility Platform Incorporating Structures for Lossless Ion Manipulation. *J. Am. Soc. Mass Spectrom.* **2021**, *32* (4), 1126−1137.
(71) Giles, K.; Ujma, J.; Wildgoose, J.; Pringle, S.; Richardson, K.; Langridge, D.; Green, M. A Cyclic Ion Mobility-Mass Spectrometry System. *Anal. Chem.* **2019**, *91* (13), 8564−8573.

https://doi.org/10.1021/jasms.1c00144
J. Am. Soc. Mass Spectrom. 2021, 32, 2621−2630